J|A|C|S
ARTICLES
Published on Web 02/28/2002

# Olefin Cis-Dihydroxylation versus Epoxidation by Non-Heme Iron Catalysts: Two Faces of an $Fe^{III}$−OOH Coin

Kui Chen, Miquel Costas, Jinheung Kim, Adrianne K. Tipton, and Lawrence Que, Jr.*

*Contribution from the Department of Chemistry and Center for Metals in Biocatalysis, University of Minnesota, Minneapolis, Minnesota 55455*

Received August 20, 2001

***Abstract:*** The oxygenation of carbon−carbon double bonds by iron enzymes generally results in the formation of epoxides, except in the case of the Rieske dioxygenases, where *cis*-diols are produced. Herein we report a systematic study of olefin oxidations with $H_2O_2$ catalyzed by a group of non-heme iron complexes, i.e., $[Fe^{II}(BPMEN)(CH_3CN)_2]^{2+}$ (**1**, BPMEN = *N,N*′-dimethyl-*N,N*′-bis(2-pyridylmethyl)-1,2-diaminoethane) and $[Fe^{II}(TPA)(CH_3CN)_2]^{2+}$ (**4**, TPA = tris(2-pyridylmethyl)amine) and their 6- and 5-methyl-substituted derivatives. We demonstrate that olefin epoxidation and cis-dihydroxylation are different facets of the reactivity of a common $Fe^{III}$−OOH intermediate, whose spin state can be modulated by the electronic and steric properties of the ligand environment. Highly stereoselective epoxidation is favored by catalysts with no more than one 6-methyl substituent, which give rise to low-spin $Fe^{III}$−OOH species (category A). On the other hand, cis-dihydroxylation is favored by catalysts with more than one 6-methyl substituent, which afford high-spin $Fe^{III}$−OOH species (category B). For catalysts in category A, both the epoxide and the *cis*-diol product incorporate $^{18}O$ from $H_2{}^{18}O$, results that implicate a *cis*-$H^{18}O$−$Fe^{V}$═O species derived from O−O bond heterolysis of a *cis*-$H_2{}^{18}O$−$Fe^{III}$−OOH intermediate. In contrast, catalysts in category B incorporate both oxygen atoms from $H_2{}^{18}O_2$ into the dominant *cis*-diol product, via a putative $Fe^{III}$-$\eta^2$-OOH species. Thus, a key feature of the catalysts in this family is the availability of two cis labile sites, required for peroxide activation. The olefin epoxidation and cis-dihydroxylation studies described here not only corroborate the mechanistic scheme derived from our earlier studies on alkane hydroxylation by this same family of catalysts (Chen, K.; Que, L, Jr. *J. Am. Chem. Soc.* **2001**, *123*, 6327) but also further enhance its credibility. Taken together, these reactions demonstrate the catalytic versatility of these complexes and provide a rationale for Nature's choice of ligand environments in biocatalysts that carry out olefin oxidations.

The oxygen activation mechanisms for hydrocarbon oxidations by heme and non-heme iron catalysts have continued to fascinate bioinorganic chemists for many years.[1−4] Understanding such mechanisms may lead to new insights in biocatalysis and drug design as well as the development of new approaches for industrial catalysis. Nature has evolved iron enzymes that carry out alkane hydroxylation, olefin epoxidation, and olefin cis-dihydroxylation. The first two transformations are carried out by catalysts with either heme (e.g., cytochrome P450)[1] or non-heme iron centers (e.g., bleomycin, methane monooxygenase),[2,3] while cis-dihydroxylation is thus far a unique activity of the non-heme iron-containing Rieske dioxygenases, which attack arene double bonds in the first step of the biodegradation of arenes by soil bacteria.[5]

Cytochrome P450 serves as the paradigm of $O_2$ activation by iron enzymes;[1] its mechanism of action is generally accepted to involve a (porphyrin radical)$Fe^{IV}$═O species,[6,7] although recent evidence has raised the possibility that a (porphyrin)-$Fe^{III}$−OOH species can also be the oxidant in some instances.[8−13] The proposed mechanisms for non-heme iron enzymes generally follow the heme paradigm. For methane monooxygenase, an $Fe^{IV}{}_2(\mu\text{-O})_2$ intermediate is proposed to be the analogue of the (porphyrin radical)$Fe^{IV}$═O oxidant,[14] while an $Fe^{III}$−OOH

(1) Sono, M.; Roach, M. P.; Coulter, E. D.; Dawson, J. H. *Chem. Rev.* **1996**, *96*, 2841−2887.
(2) Wallar, B. J.; Lipscomb, J. D. *Chem. Rev.* **1996**, *96*, 2625−2658.
(3) Que, L., Jr.; Ho, R. Y. N. *Chem. Rev.* **1996**, *96*, 2607−2624.
(4) Solomon, E. I.; Brunold, T. C.; Davis, M. I.; Kemsley, J. N.; Lee, S.-K.; Lehnert, N.; Neese, F.; Skulan, A. J.; Yang, Y.-S.; Zhou, J. *Chem. Rev.* **2000**, *100*, 235−349.
(5) Gibson, D. T. *Microbial Degradation of Organic Compounds*; Marcel Dekker: New York, 1984.
(6) Groves, J. T.; Han, Y.-Z. In *Cytochrome P450: Structure, Mechanism, and Biochemistry*, 2nd ed.; Ortiz de Montellano, P. R., Ed.; Plenum Press: New York, 1995; pp 3−48.
(7) Schlichting, I.; Berendzen, J.; Chu, K.; Stock, A. M.; Maves, S. A.; Benson, D. E.; Sweet, R. M.; Ringe, D.; Petsko, G. A.; Sligar, S. G. *Science* **2000**, *287*, 1615−1622.
(8) Pratt, J. M.; Ridd, T. I.; King, L. J. *Chem. Commun.* **1995**, 2297−2298.
(9) Vaz, A. D. N.; Pernecky, S. J.; Raner, G. M.; Coon, M. J. *Proc. Natl. Acad. Sci. U.S.A.* **1996**, *93*, 4644−4648.
(10) Lee, K. A.; Nam, W. *J. Am. Chem. Soc.* **1997**, *119*, 1916−1922.
(11) Newcomb, M.; Toy, P. H. *Acc. Chem. Res.* **2000**, *33*, 449−455.
(12) Nam, W.; Lim, M. H.; Lee, H. J.; Kim, C. *J. Am. Chem. Soc.* **2000**, *122*, 6641−6647.
(13) Nam, W.; Lim, M. H.; Moon, S. K.; Kim, C. *J. Am. Chem. Soc.* **2000**, *122*, 10805−10809.
(14) Shu, L.; Nesheim, J. C.; Kauffmann, K.; Münck, E.; Lipscomb, J. D.; Que, L., Jr. *Science* **1997**, *275*, 515−518.


**10.1021/ja0120025 CCC: $22.00** 

***Chart 1.*** Ligands Used in This Study and the Numbering Scheme for Corresponding Iron Complexes

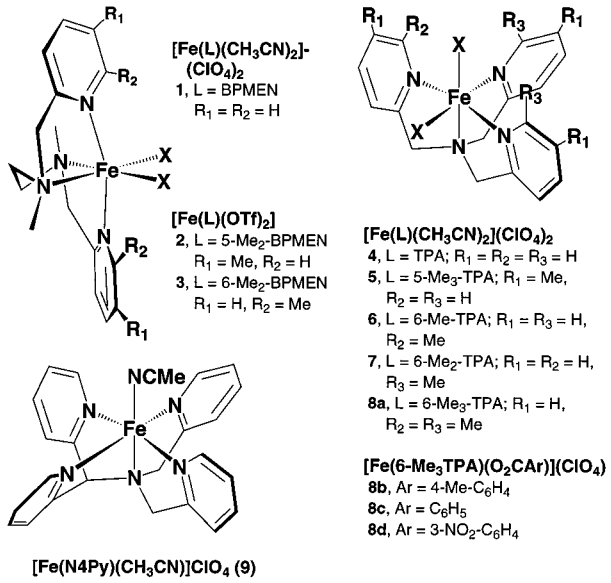


intermediate has been observed in the reaction cycle of the antitumor drug bleomycin.[15−18] These intermediates are believed to be involved in the hydroxylation of aliphatic C−H bonds and the epoxidation of C−C double bonds.

On the other hand, scant insight is available for the cis-dihydroxylation of C−C double bonds by Rieske dioxygenases, where both oxygen atoms of $O_2$ are incorporated into the product.[5] The active site of naphthalene 1,2-dioxygenase consists of a mononuclear iron center coordinated by two histidines and a bidentate carboxylate group, with the remaining two cis sites available for exogenous ligand binding.[19] Evidence for an iron−peroxo intermediate is suggested by the crystal structure of a putative indole−dioxygen adduct bound to the mononuclear iron center,[20] but no intermediates have been detected spectroscopically in the catalytic cycle of these enzymes.[21] To date, mechanistic speculations center on the involvement of $Fe^{III}$-$\eta^2$-peroxo or HO−$Fe^{V}$═O species.[3,21]

In the course of developing functional models for non-heme iron oxygenases, we have discovered a family of non-heme iron catalysts (Chart 1) that are capable of stereospecific hydrocarbon oxidations with $H_2O_2$ as the oxidant. We have reported a detailed mechanistic study of stereospecific alkane hydroxylation by this family of catalysts and found evidence for the participation of an $Fe^{V}$═O species.[22] Here we present a systematic study of olefin oxidation by these catalysts. Although examples of olefin epoxidation with $H_2O_2$ by non-heme iron catalysts are known,[23,24] the complexes studied here represent the first examples of iron catalysts capable of olefin cis-dihydroxylation. In this study, we provide strong mechanistic evidence for the involvement of a formally non-heme iron(V)−oxo species in these reactions and demonstrate that olefin epoxidation and cis-dihydroxylation activities derive from a common $Fe^{III}$−OOH intermediate whose properties and reactivity can be tuned by the ligand environment. Some aspects of this work have been published previously as communications.[25−27]

## Experimental Section

**Materials and Syntheses.** All reagents were purchased from Aldrich and used as received unless noted otherwise. $H_2{}^{18}O$ (85 or 96.5% $^{18}O$-enriched), $H_2{}^{18}O_2$ (90% $^{18}O$-enriched, 2% solution in $H_2{}^{16}O$), and $^{18}O_2$ (96% $^{18}O$-enriched) were obtained from ICON. $H_2{}^{18}O$ (88.8 or 98.6% $^{18}O$-enriched) was obtained from Isotec. Cyclooctene was purified by vacuum distillation, while other olefins were purified by passing through silica gel immediately before the reactions. The epoxides of *cis*- and *trans*-2-heptenes were obtained from stereospecific epoxidation by *m*-chloroperoxybenzoic acid, and the corresponding diols were from the hydrolysis of the epoxides.

The syntheses of all complexes used in this study except for **2** and **3** have been previously reported; these complexes and corresponding references are listed as follows: $[Fe^{II}(BPMEN)(CH_3CN)_2](ClO_4)_2$ (**1**),[28] $[Fe^{II}(TPA)(CH_3CN)_2](ClO_4)_2$ (**4**),[29] $[Fe^{III}{}_2O(TPA)_2(H_2O)_2](ClO_4)_4$ (**4a**),[30] $[Fe^{II}(5\text{-}Me_3\text{-}TPA)(CH_3CN)_2](ClO_4)_2$ (**5**),[22] $[Fe^{II}(6\text{-}Me_n\text{-}TPA)(CH_3CN)_2](ClO_4)_2$ (**6**, $n = 1$; **7**, $n = 2$; **8a**, $n = 3$),[29] $[Fe^{II}(6\text{-}Me_3\text{-}TPA)(O_2CC_6H_4X)](ClO_4)$ (**8b**, X = 4-Me; **8c**, X = H; **8d**, X = 3-$NO_2$),[31] and $[Fe^{II}(N4Py)(CH_3CN)](ClO_4)_2$ (**9**).[32] *Caution: Perchlorate salts are potentially explosive and should be handled with care.*

Complexes **2** and **3** were synthesized by mixing equimolar amounts of $Fe^{II}(OTf)_2{\cdot}2CH_3CN$ (OTf = trifluoromethanesulfonate) and the tetradentate ligand in THF solution to afford a precipitate after a few minutes of stirring. The precipitate was dissolved in $CH_2Cl_2$ and layered with hexane to afford the products as yellow (**2**) or white (**3**) crystalline solids upon standing at −20 °C for 3 days under Ar. Elemental analyses were performed by Atlantic Microlab (Norcross, GA). $[Fe^{II}(5\text{-}Me_2\text{-}BPMEN)(OTf)_2]$ **(2)**. Anal. Calcd (found) for $C_{20}H_{26}F_6FeN_4O_6S_2{\cdot}0.5H_2O$: C, 36.32 (36.13); H, 4.11 (3.94); N, 8.47 (8.40). $[Fe^{II}(6\text{-}Me_2\text{-}BPMEN)(OTf)_2]$ **(3).** Anal. Calcd (found) for $C_{20}H_{26}F_6FeN_4O_6S_2{\cdot}0.5H_2O$: C, 36.32 (36.15); H, 4.11 (4.07); N, 8.47 (8.38).

**Crystallographic Studies.** Crystals suitable for crystallographic analysis were obtained from $CH_2Cl_2$/hexane for **2** and from $CH_2Cl_2$/diethyl ether for **3**. Data collection and analysis were conducted on a Siemens SMART system at the X-ray Crystallographic Laboratory of the Chemistry Department of the University of Minnesota. Pertinent crystallographic data and experimental conditions are summarized in Table S1 (Supporting Information). The structures were solved by direct methods using the SHELXTL V5.0 suite of programs. All non-hydrogen atoms were refined anisotropically, and hydrogen atoms were placed in ideal positions and refined as riding atoms with individual (or group if appropriate) isotropic displacement parameters.

**Instrumentation.** $^1H$ NMR spectra were recorded on a Varian Unity 300 or 500 spectrometer at ambient temperature. Chemical shifts (ppm)

(15) Stubbe, J.; Kozarich, J. W. *Chem. Rev.* **1987**, *87*, 1107−1136.
(16) Sam, J. W.; Tang, X.-J.; Peisach, J. *J. Am. Chem. Soc.* **1994**, *116*, 5250−5256.
(17) Burger, R. M. *Struct. Bonding* **2000**, *97*, 287−303.
(18) Neese, F.; Zaleski, J. M.; Zaleski, K. L.; Solomon, E. I. *J. Am. Chem. Soc.* **2000**, *122*, 11703−11724.
(19) Kauppi, B.; Lee, K.; Carredano, E.; Parales, R. E.; Gibson, D. T.; Eklund, H.; Ramaswamy, S. *Structure* **1998**, *6*, 571−586.
(20) Carredano, E.; Karlsson, A.; Kauppi, B.; Choudhury, D.; Parales, R. E.; Parales, J. V.; Lee, K.; Gibson, D. T.; Eklund, H.; Ramaswamy, S. *J. Mol. Biol.* **2000**, *296*, 701−712.
(21) Wolfe, M. D.; Parales, J. V.; Gibson, D. T.; Lipscomb, J. D. *J. Biol. Chem.* **2001**, *276*, 1945−1953.
(22) Chen, K.; Que, L., Jr. *J. Am. Chem. Soc.* **2001**, *123*, 6327−6337.
(23) Nam, W.; Ho, R. Y. N.; Valentine, J. S. *J. Am. Chem. Soc.* **1991**, *113*, 7052−7054.
(24) Guajardo, R. J.; Hudson, S. E.; Brown, S. J.; Mascharak, P. K. *J. Am. Chem. Soc.* **1993**, *115*, 7971−7977.
(25) Kim, C.; Chen, K.; Kim, J.; Que, L., Jr. *J. Am. Chem. Soc.* **1997**, *119*, 5964−5965.
(26) Chen, K.; Que, L., Jr. *Angew. Chem., Int. Ed. Engl.* **1999**, *38*, 2227−2229.
(27) Costas, M.; Tipton, A. K.; Chen, K.; Jo, D.-H.; Que, L., Jr. *J. Am. Chem. Soc.* **2001**, *123*, 6722−6723.
(28) Chen, K.; Que, L., Jr. *Chem. Commun.* **1999**, 1375−1376.
(29) Zang, Y.; Kim, J.; Dong, Y.; Wilkinson, E. C.; Appelman, E. H.; Que, L., Jr. *J. Am. Chem. Soc.* **1997**, *119*, 4197−4205.
(30) Dong, Y.; Fujii, H.; Hendrich, M. P.; Leising, R. A.; Pan, G.; Randall, C. R.; Wilkinson, E. C.; Zang, Y.; Que, L., Jr.; Fox, B. G.; Kauffmann, K.; Münck, E. *J. Am. Chem. Soc.* **1995**, *117*, 2778−2792.
(31) Kim, J.; Zang, Y.; Costas, M.; Harrison, R. G.; Wilkinson, E. C.; Que, L., Jr. *J. Biol. Inorg. Chem.* **2001**, *6*, 276−284.
(32) Lubben, M.; Meetsma, A.; Wilkinson, E. C.; Feringa, B.; Que, L., Jr. *Angew. Chem., Int. Ed. Engl.* **1995**, *34*, 1512−1514.

were referenced to the residual protic solvent peaks. Electrospray ionization mass spectral experiments were carried out on a Sciex API III mass spectrometer (Sciex, Thornhill, ON, Canada).[33] Product analyses were performed on a Perkin-Elmer Sigma 3 gas chromatograph (AT-1701 column, 30 m) with a flame ionization detector. GC mass spectral analyses were performed on a HP 5898 GC (DB-5 column, 60 m) with a Finnigan MAT 95 mass detector or a HP 6890 GC (HP-5 column, 30 m) with an Agilent 5973 mass detector. A 4% $NH_3/CH_4$ mix was used as the ionization gas for chemical ionization analyses.

**Reaction Conditions for Catalytic Oxidations.** In a typical reaction, 0.3 mL of a 70 mM $H_2O_2$ solution (diluted from a 35 or 50% $H_2O_2$ solution) in $CH_3CN$ was delivered by syringe pump over 30 min at 25 °C in air to a vigorously stirred $CH_3CN$ solution (2.7 mL) containing iron catalyst and olefin substrate. The final concentrations were 0.7 mM mononuclear iron catalyst (or 0.35 mM dinuclear iron catalyst **4a**), 7.0 mM $H_2O_2$, and 0.70 M olefin. The solution was stirred for another 5 min after syringe pump addition was complete. The organic products were either directly extracted into diethyl ether solution or esterified by 1 mL of acetic anhydride together with 0.1 mL of 1-methylimidazole[34] followed by $CHCl_3$ extraction. To the organic extract was added an internal standard and the solution was subjected to GC analysis. The products were identified by comparison of their GC retention times, GC/MS, and $^1H$ and $^{13}C$ NMR spectra with those of authentic compounds.

**Isotope Labeling Studies.** Similar conditions as described above were used for isotope labeling studies except for the following details. In experiments with $H_2{}^{18}O$, 42 $\mu$L of $H_2{}^{18}O$ (0.70 M) was added to the catalyst solution prior to the injection of $H_2O_2$. In experiments with $H_2{}^{18}O_2$, 7.0 mM $H_2{}^{18}O_2$ (diluted by $CH_3CN$ from a 2% $H_2{}^{18}O_2/H_2O$ solution) was used instead of $H_2O_2$. The organic products were subjected to GC/CI-MS analyses. All labeling experiments were run at least in duplicate. The data reported were the average of these reactions and calculated on the basis of the $^{18}O$-enrichment of the reagents containing the isotope.

## Results

In a recent paper, we reported an investigation of a series of non-heme iron(II) complexes with respect to their ability to catalyze alkane hydroxylation with $H_2O_2$ as oxidant and found a number of these carry out stereospecific hydroxylation.[22] In this paper, we focus on a similar series of catalysts and their ability to oxidize olefins. All complexes in this study are six-coordinate with a tetradentate N4 ligand based on either the tripodal tris(2-pyridylmethyl)amine (TPA) or the linear *N*,*N*′-dimethyl-*N*,*N*′-bis(2-pyridylmethyl)-1,2-diaminoethane (BPMEN) framework (Chart 1). The remaining coordination sites are occupied by labile ligands such as $CH_3CN$, trifluoromethanesulfonate (OTf), or benzoate.

**Physical Properties of the Catalysts.** Several of the complexes have been crystallographically characterized.[22,28,29,31] Exemplifying the family of TPA-based complexes, **4**, **5**, **8a**, and **8c** have two cis coordination sites for $CH_3CN$ or benzoate. This geometry is also maintained in the BPMEN family of complexes. Although the BPMEN ligand can in principle adopt three possible conformations, only one of these is observed for complexes **1**−**3** (Figure 1). The tetradentate ligand adopts a cis-α conformation with the two pyridine rings coordinated to the metal center trans to each other. While we were not able to crystallize the bis(acetonitrile) derivatives of **2** and **3**, we were successful with the corresponding bis(triflate) complexes, and

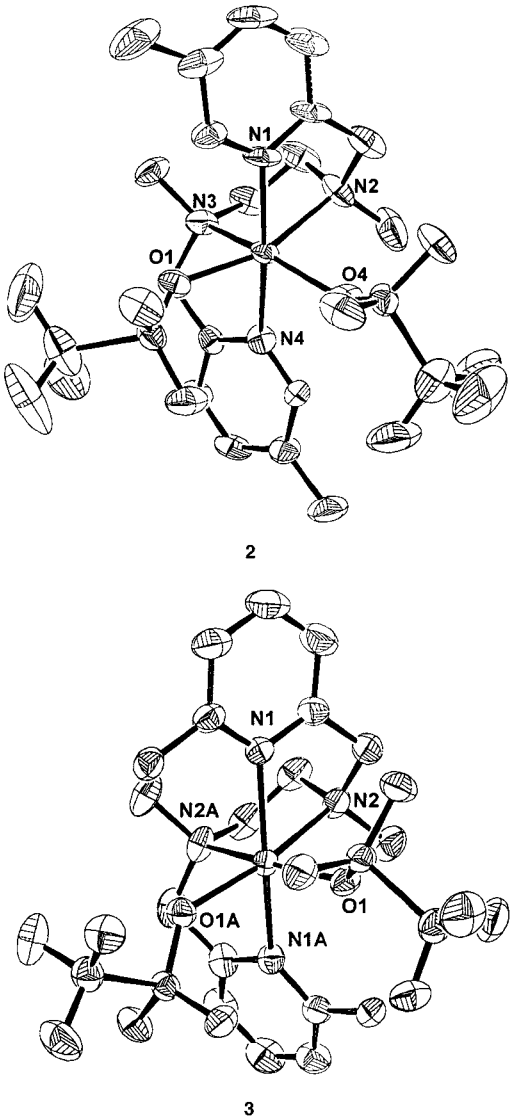


***Figure 1.*** ORTEP plots for [Fe(5-$Me_2$-BPMEN)$(OTf)_2$] (**2**) and [Fe(6-$Me_2$-BPMEN)$(OTf)_2$] (**3**) showing 50% probability ellipsoids. Hydrogen atoms omitted for clarity.

crystallographic data for these two complexes can be found in the Supporting Information. The cis-α conformation favored by the BPMEN family of ligands in these complexes requires the two remaining ligands, either $CH_3CN$ or OTf, to occupy sites that are cis to each other, as in the TPA family of complexes.

From their solid-state structures, it can be deduced that **4** and **5**, representing the TPA and 5-$Me_3$-TPA complexes, respectively, have low-spin iron(II) centers, with Fe−N bond lengths of less than 2 Å (Table 1). The parent BPMEN complex, **1**, is similar but with slightly longer Fe−N bond lengths (Table 1). The other structurally characterized complexes are high spin, with Fe−N bond lengths averaging 2.2 Å (Table 1). This change in spin state is due either to the replacement of $CH_3CN$ with the much weaker triflate ligand or to the introduction of a 6-Me substituent on the pyridine ring. Although the presence of a 6-methyl group may be expected to make the pyridine ligand a stronger $\sigma$-donor and favor the low-spin state, steric repulsion between the methyl group and the metal center prevents the formation of the shorter Fe−N bonds required for the low-spin state and overcomes the donating effect to favor the high-spin configuration.[29,35−37]

(33) Kim, J.; Dong, Y.; Larka, E.; Que, L., Jr. *Inorg. Chem.* **1996**, *35*, 2369−2372.
(34) Elvebak, L. E., II.; Schmitt, T.; Gary, G. R. *Carbohydr. Res.* **1993**, *246*, 1−11.

***Table 1.*** Selected Bond Lengths (Å) for $[Fe^{II}(BPMEN)(CH_3CN)_2]^{2+}$ (**1**), $[Fe^{II}(5\text{-}Me_2\text{-}BPMEN)(OTf)_2]$ (**2**), $[Fe^{II}(6\text{-}Me_2\text{-}BPMEN)(OTf)_2]$ (**3**), $[Fe^{II}(TPA)(CH_3CN)_2]^{2+}$ (**4**), $[Fe^{II}(5\text{-}Me_3\text{-}TPA)(CH_3CN)_2]^{2+}$ (**5**), and $[Fe^{II}(6\text{-}Me_3\text{-}TPA)(CH_3CN)_2]^{2+}$ (**8a**)

| | **1**[a] | **2**(A)[b] | **2**(B)[b] | 3 | **4**[c] | **5**[d] | **8a**[e] |
|---|---|---|---|---|---|---|---|
| $Fe-N_{amine}$ | 2.055(5) | 2.214(5) | 2.210(4) | 2.2189(19) | 1.99(1) | 1.998(3) | 2.15(1) |
| | 2.053(5) | 2.228(5) | 2.232(5) | 2.2189(19) | | | |
| $Fe-N_{pyridine}$ | 2.002(4) | 2.162(4) | 2.196(4) | 2.2899(19) | 1.97(1) | 1.984(3) | 2.25(1) |
| | 2.015(4) | 2.175(4) | 2.184(4) | 2.2900(19) | 1.92(1) | 1.969(3) | 2.18(1) |
| | | | | | 1.95(1) | 1.985(3) | 2.24(1) |
| $Fe-N_{acetonitrile}$ | 1.942(5) | | | | 1.92(1) | 1.960(3) | 2.17(1) |
| | 1.950(5) | | | | 1.93(1) | 1.948(3) | 2.17(1) |
| $Fe-O_{triflate}$ | | 2.090(4) | 2.082(7) | 2.1061(15) | | | |
| | | 2.127(4) | 2.160(4) | 2.1062(15) | | | |

[a] Reference 28. [b] Two crystallographically distinct molecules in the unit cell. [c] Reference 29. [d] Reference 22. [e] Reference 31.

***Table 2.*** Oxidation of Cyclooctene by $H_2O_2$ Catalyzed by Iron Complexes[a]

| | catalyst | *cis*-diol[b] | oxide[b] | *cis*-diol:oxide | conv[c] (%) |
|---|---|---|---|---|---|
| **1** | $[Fe(BPMEN)(CH_3CN)_2]^{2+}$ | 0.9(2) | 7.5(6) | 1:8 | 84 |
| **2** | $[Fe(5\text{-}Me_2\text{-}BPMEN)(OTf)_2]$ | 1.3(4) | 7.8(3) | 1:6 | 91 |
| **3** | $[Fe(6\text{-}Me_2\text{-}BPMEN)(OTf)_2]$ | 6.2(1)[d] | 1.5(1) | 4:1 | 79 |
| **4** | $[Fe(TPA)(CH_3CN)_2]^{2+}$ | 4.0(2) | 3.4(1) | 1.2:1 | 74 |
| **4a** | $[Fe_2O(TPA)_2(H_2O)_2]^{4+}$ | 4.1(1) | 4.0(1) | 1:1 | 81 |
| **5** | $[Fe(5\text{-}Me_3\text{-}TPA)(CH_3CN)_2]^{2+}$ | 3.9(4) | 2.8(1) | 1.4:1 | 67 |
| **6** | $[Fe(6\text{-}Me\text{-}TPA)(CH_3CN)_2]^{2+}$ | 2.8(1) | 2.1(2) | 1.3:1 | 49 |
| **7** | $[Fe(6\text{-}Me_2\text{-}TPA)(CH_3CN)_2]^{2+}$ | 5.5(1) | 1.1(2) | 5:1 | 66 |
| **8a** | $[Fe(6\text{-}Me_3\text{-}TPA)(CH_3CN)_2]^{2+}$ | 4.9(6) | 0.7(2) | 7:1 | 56 |
| **8b** | $[Fe(6\text{-}Me_3\text{-}TPA)(O_2CC_6H_4\text{-}4\text{-}Me)]^{+}$ | 5.0(6) | 0.5(1) | 10:1 | 55 |
| **8c** | $[Fe(6\text{-}Me_3\text{-}TPA)(O_2CC_6H_5)]^{+}$ | 6.1(4) | 0.5(1) | 12:1 | 66 |
| **8d** | $[Fe(6\text{-}Me_3\text{-}TPA)(O_2CC_6H_4\text{-}3\text{-}NO_2)]^{+}$ | 6.7(3) | 0.4(1) | 17:1 | 71 |
| **9** | $[Fe(N4Py)(CH_3CN)]^{2+}$ [26] | 0 | 0.6 | | 6 |
| **10** | $[Fe(cyclam)(OTf)_2]$[e] [23] | 0 | 4 | | 40 |
| **11** | [Fe(TMP)Cl][e] [39] | 0 | 0.2 | | 2 |
| **12** | $[Fe(F_{20}TPP)Cl]$[e] [39] | 0 | 8.6 | | 86 |

[a] See Experimental Section for reaction conditions. [b] Yields expressed in moles of product per mole of iron. [c] Percent conversion of $H_2O_2$ into epoxide and *cis*-diol products. [d] 0.2(1) TN of *trans*-diol also observed. [e] Values scaled to 10 equiv of $H_2O_2$ for comparison; cyclam = 1,4,8,11-tetraazacyclotetradecane; TMP = tetramesitylporphinato dianion; $F_{20}$TPP = tetrakis(pentafluorophenyl)porphinato dianion.

In general, the complexes maintain their spin states in $CH_3CN$ solution, as determined by $^1$H NMR spectroscopy. Thus, **4** and **5** exhibit spectra with a compact NMR shift range of 0−12 ppm, as expected for diamagnetic complexes, while **2**, **3**, **6**, **7**, and **8a**−**d** exhibit spectra typical of high-spin Fe(II) complexes with shifts that range from 120 to −50 ppm. Consistent with its crystal structure, **1** exhibits a compact $^1$H NMR spectrum expected of a diamagnetic complex, but only at −40 °C. The shifts increase monotonically with an increase in temperature such that a spectrum spanning 90 ppm in chemical shift is observed at 30 °C, indicating that the iron(II) center undergoes a transition from low spin to high spin in this temperature range.

**Catalyst Efficiency.** Table 2 summarizes the results of cyclooctene oxidation experiments catalyzed by complexes **1**−**8**. All catalytic oxidation experiments were performed in air at ambient temperature by delivery of 10 equiv of $H_2O_2$ via syringe pump over a 30-min period. For **4**, the yields of epoxide and *cis*-diol were unaffected by the presence of air. $H_2O_2$ was introduced by syringe pump in order to minimize disproportionation of the peroxide that may be catalyzed by the iron complex (catalase side reaction). For example, when the 10 equiv of $H_2O_2$ were added all at once in the case of **4**, the yields of cyclooctene oxidation products decreased by 50%, from 7.4 to 3.8 turnovers (mol of product/mol of catalyst). Iodometric titrations of the solutions at the end of the reaction indicated that all the peroxide had been consumed. A perusal of Table 2 shows that 49−91% of the $H_2O_2$ was converted into olefin oxidation products, depending on the catalyst used. Thus, compared to other iron catalysts in the literature, the complexes studied here have among the best conversion efficiencies for the oxidation of cyclooctene with $H_2O_2$ (Table 2). Furthermore **1**−**3**, with ligands based on an ethylenediamine backbone, are somewhat more effective in converting $H_2O_2$ into oxidation products than their TPA counterparts. This difference in conversion efficiency has also been observed under similar conditions in alkane hydroxylation reactions.[22,28]

The products of cyclooctene oxidation are almost exclusively the corresponding epoxide and *cis*-diol. The appearance of the *cis*-diol product was unexpected in the initial stages of this work, as cis-dihydroxylation of olefins had not previously been observed for iron catalysts and is a reaction more commonly associated with high-valent second and third row metal centers with a *cis*-dioxometal motif. However *cis*-cyclooctane-1,2-diol can be unambiguously identified on the basis of its $^1$H NMR spectrum and GC/MS profile in comparison with the authentic compound. Control experiments demonstrated that the diol did not come from the epoxide under the same experimental conditions. Hydrolytic cleavage of the epoxide ring should only give the *trans*-diol, and no *trans*-diol was found for any of the oxidation experiments except for the small amounts observed in the case of **3**. These complexes thus represent the first examples of iron catalysts capable of olefin cis-dihydroxylation.

Many of these catalysts are robust and maintain their ability to catalyze olefin oxidation with more equivalents of $H_2O_2$ (Table 3). For example, for **1**, the 75% conversion of $H_2O_2$ to epoxide is maintained with the addition of 20 and 40 equiv of $H_2O_2$, affording 15 and 29 total turnovers of epoxide products, respectively. Thus, **1** is an excellent epoxidation catalyst, an observation that was also reported recently by White et al.[38] Similarly, for **8a** and **8d**, the respective 50 and 70% conversions of $H_2O_2$ to *cis*-diol are maintained with the addition of 20 and 40 equiv od $H_2O_2$; these complexes are therefore excellent catalysts for olefin cis-dihydroxylation.

Complexes **1**−**8** differ significantly from $[Fe(N4Py)(CH_3CN)]^{2+}$ (**9**), $[Fe(cyclam)(OTf)_2]$ (cyclam = 1,4,8,11-tetraazacyclotetradecane), and iron porphyrin complexes with respect

(35) Gütlich, P. *Struct. Bonding* **1981**, *44*, 83−195.
(36) Gütlich, P.; Hauser, A.; Spiering, H. *Angew. Chem., Int. Ed. Engl.* **1994**, *33*, 2024−2054.
(37) Constable, E. C.; Baum, G.; Bill, E.; Dyson, R.; Eldik, R. v.; Fenske, D.; Kaderli, S.; Morris, D.; Neubrand, A.; Neuburger, M.; Smith, D. R.; Wieghardt, K.; Zehnder, M.; Zuberbühler, A. D. *Chem. Eur. J.* **1999**, *5*, 498−508.
(38) White, M. C.; Doyle, A. G.; Jacobsen, E. N. *J. Am. Chem. Soc.* **2001**, *123*, 7194−7195.

***Table 3.*** Oxidation of Cyclooctene by $H_2O_2$ Catalyzed by Selected Iron Complexes[a]

| catalyst | $H_2O_2$ (equiv) | *cis*-diol[b] | oxide[b] | *cis*-diol:oxide | conv[c] (%) |
|---|---|---|---|---|---|
| **1** | 10 | 0.9(2) | 7.5(6) | 1:8 | 84 |
| | 20 | 1.4(1) | 15(1) | 1:10 | 82 |
| | 40 | 2.2(2) | 29(1) | 1:13 | 78 |
| **4** | 10 | 4.0(2) | 3.4(2) | 1.2:1 | 74 |
| | 20 | 8.3(2) | 5.8(2) | 1.4:1 | 70 |
| | 40 | 14.9(6) | 10.3(2) | 1.4:1 | 63 |
| **8a** | 10 | 4.9(6) | 0.7(2) | 7:1 | 56 |
| | 20 | 10(2) | 0.8(1) | 12:1 | 54 |
| | 40 | 22(1) | 1.6(1) | 14:1 | 59 |
| **8d** | 10 | 6.7(3) | 0.4(1) | 16:1 | 71 |
| | 20 | 15(1) | 0.8(1) | 19:1 | 79 |
| | 40 | 28(1) | 1.8(1) | 16:1 | 75 |

[a] See Experimental Section for reaction conditions. [b] Yields expressed in moles of product per mole of iron. [c] Percent conversion of $H_2O_2$ into epoxide and *cis*-diol products.

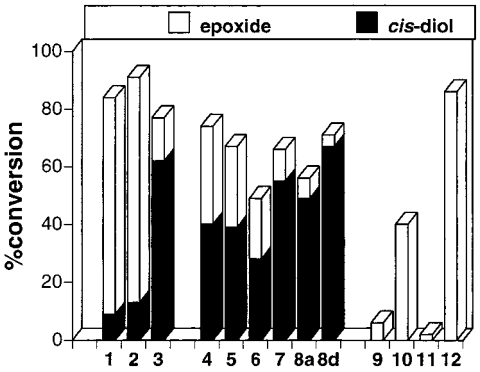


***Figure 2.*** Percent conversion of $H_2O_2$ into epoxide and *cis*-diol products derived from cyclooctene oxidation catalyzed by complexes **1**−**12** based on data listed in Table 2. See Chart 1 for structures of complexes **1**−**9**; **10** = [Fe(cyclam)(OTf)$_2$]; **11** = [Fe(TPP)Cl]; **12** = [Fe($F_{20}$TPP)Cl].

to their ability to catalyze olefin oxidations *with $H_2O_2$ as oxidant* (Table 1). Complex **9** has a pentadentate ligand that differs from TPA in having an additional pendant pyridine, but unlike **4**, it is a rather poor catalyst for olefin oxidation.[26] On the other hand, complexes of tetradentate macrocyclic ligands such as cyclam[23] and porphyrins[12,39,40] catalyze olefin epoxidation but not cis-dihydroxylation. A structural element that distinguishes **1**−**8** from the other complexes is the fact that these complexes all have two cis labile coordination sites. As in our earlier study of stereospecific alkane hydroxylation by this family of complexes,[22] we will argue that this feature plays a key role in the olefin oxidation catalysis observed.

**Ligand Tuning of the *cis*-Diol-to-Epoxide Ratio.** As shown in Table 2 and illustrated in Figure 2, the *cis*-diol/epoxide ratio depends dramatically on the nature of the iron catalyst employed. Complexes **1** and **2** afford predominantly epoxide product, with diol/epoxide ratios of 1:8 and 1:6, respectively. In contrast, the corresponding 6-methyl-substituted analogue **3** converts only 15% of the $H_2O_2$ added to epoxide and 62% to diol for a diol/epoxide ratio of 4:1. Thus, the introduction of 6-methyl groups on the pyridine rings results in a 32-fold change in the selectivity of the oxidation from epoxidation to cis-dihydroxylation.

The TPA series **4**−**8** exhibits a less dramatic change in product ratios but nevertheless emphasizes the significant effect of adding 6-methyl substituents (Table 2 and Figure 2). Complex **4** affords a *cis*-diol/epoxide ratio of 1.2:1, a ratio that increases only slightly with the introduction of either three 5-methyl substituents (**5**) or one 6-methyl group (**6**). However, the addition of a second (**7**) and a third 6-methyl group (**8a**) causes the ratio to jump to 5 and 7, respectively. The high selectivity of **8a** for the *cis*-diol product is further improved when the two $CH_3CN$ ligands are replaced with a bidentate benzoate (**8b**−**d**). In fact, the *cis*-diol accounts for 95% of the overall oxidation product when *m*-nitrobenzoate is used, making **8d** the most selective iron catalyst reported to date for the cis-dihydroxylation of olefins.[41]

Table 4 shows that the ligand preferences for olefin epoxidation versus cis-dihydroxylation observed for cyclooctene are maintained for a variety of olefinic substrates. As noted earlier, **1** is primarily an epoxidation catalyst, while **3** and **8d** strongly favor cis-dihydroxylation, with **4** exhibiting an olefin oxidation preference that is intermediate between these two extremes. Thus, a small modification of the architecture of the complex, represented in this series by the introduction of 6-methyl substituents on the pyridine ligands, allows the exquisite tuning of the oxidative reactivity exhibited by the iron catalyst.

**Stereoselectivity.** A more detailed study of the oxidation of the isomeric *cis*- and *trans*-2-heptenes reveals a significant ligand dependence on the stereoselectivity of the reactions (Table 5). With respect to epoxidation, all the complexes convert *trans*-2-heptene stereospecifically to the corresponding *trans*-epoxide with RC values of greater than 99% (RC = 100(cis − trans)/(cis + trans) or 100(trans − cis)/(cis + trans) for *cis*- or *trans*-olefins, respectively). More discriminating is the epoxidation of *cis*-2-heptene. The parent BPMEN and TPA complexes (**1** and **4**, respectively) afford the corresponding *cis*-epoxide with a high degree of stereoretention (RC values of 92 and 80%, respectively), and the results are not affected by 5-Me substitution. On the other hand, the stereoselectivity of *cis*-2-heptene epoxidation decreases dramatically with the introduction of 6-methyl substituents. For the 6-$Me_3$-TPA complexes, where the epoxide represents less than 10% of the total oxidized product, the two epoxide isomers are formed in comparable amounts. In sharp contrast, the cis-dihydroxylation of the isomeric heptenes occurs with a high degree of stereoretention for all catalysts studied. These differences show that epoxidation and cis-dihydroxylation, although related, must proceed by distinct mechanisms.

The loss of stereoselectivity in *cis*-2-heptene epoxidation suggests the participation of an oxidized olefin species capable of fast epimerization to the more stable trans isomer prior to epoxide ring formation, such as a radical cation intermediate. While not very important for the parent BPMEN and TPA catalysts, this channel becomes more predominant as the number of 6-methyl substituents on the catalyst increases. The involvement of a radical cation is also supported by the results of styrene oxidation (Table 4). Indeed PhCHO is a significant byproduct of the oxidation, which derives from $O_2$ trapping of

(39) Traylor, T. G.; Tsuchiya, S.; Byun, Y.-S.; Kim, C. *J. Am. Chem. Soc.* **1993**, *115*, 2775−2781.
(40) Bartoli, J.-F.; Le Barch, K.; Palacio, M.; Battioni, P.; Mansuy, D. *Chem. Commun.* **2001**, 1718−1719.

(41) The somewhat better conversion efficiency of **8d** compared to **8a** (67 vs 49%) is not understood. However, we note that the best catalyst among the 6-$Me_3$-TPA complexes is **8d**, the one with the least basic carboxylate ligand. We speculate that the carboxylate is displaced as the acid in the generation of the $Fe^{III}$−OOH intermediate (vide infra). At the end of the catalytic cycle, this acid protonates the bound diolate product to enhance its displacement from the metal coordination sphere and initiate another catalytic cycle.

***Table 4.*** Oxidation of Various Olefins by Selected Non-Heme Iron Catalysts[a]

| | 1 | | 3 | | 4 | | 8d | |
|---|---|---|---|---|---|---|---|---|
| olefin | diol[b] | epoxide[b] | diol[b] | epoxide[b] | diol[b] | epoxide[b] | diol[b] | epoxide[b] |
| cyclooctene | 0.9(2) | 7.5(6) | 6.4(1) | 1.5(1) | 4.0(2) | 3.4(1) | 6.7(3) | 0.4(1) |
| *cis*-2-heptene | 0.9(1) | 5.5(3) | 4.6(2) | 2.0(1) | 3.0(3) | 1.9(1) | 4.5(2) | 0.4(1) |
| *trans*-2-heptene | 0.6(1) | 5.3(1) | 2.6(2) | 1.5(3) | 3.3(3) | 1.5(1) | 5.3(1) | 0.2(1) |
| 1-octene | 1.3(1) | 4.1(1) | 5.3(1) | 0.7(1) | 5.3(3) | 2.2(1) | 5.5(2) | 0.3(2) |
| vinylcyclohexane | 1.5(2) | 5.0(2) | 5.0(2) | 2.2(2) | 5.3(3) | 2.7(1) | 5.6(2) | 0.5(1) |
| styrene | 2.0(1) | 1.1(1) | 4.8(2) | 1.6(1) | 2.4(1) | 1.7(1) | 5.2(1) | 0.6(1) |
| | | 6.4(1)[c] | | 2.2(4)[c] | | 1.6(1)[c] | | 1.9(1)[c] |

[a] See Experimental Section for reaction conditions. [b] Yields expressed in moles of product per mole of iron. [c] PhCHO byproduct observed due to autoxidation.

***Table 5.*** Oxidation of *cis*- and *trans*-2-Heptenes[a]

| | | *cis*–2-heptene | | | | *trans*–2-heptene | | | |
|---|---|---|---|---|---|---|---|---|---|
| catalyst | ligand | diol[b] | RC[c] | epoxide[b] | RC[c] | diol[b] | RC[c] | epoxide[b] | RC[c] |
| **1** | BPMEN | 0.9(1) | 79 | 5.5(3) | 92 | 0.6(1) | 88 | 5.3(1) | >99 |
| **2** | 5-$Me_2$-BPMEN | 0.9(1) | 79 | 5.2(1) | 90 | 1.1(1) | 92 | 5.1(1) | >99 |
| **3** | 6-$Me_2$-BPMEN | 4.6(2) | 78 | 2.0(1) | 60 | 2.6(2) | 95 | 1.5(3) | >99 |
| **4** | TPA | 3.0(3) | 96 | 1.9(1) | 80 | 3.3(3) | 96 | 1.5(1) | >99 |
| **5** | 5-$Me_3$-TPA | 4.4(1) | 94 | 2.3(1) | 83 | 5.2(1) | >99 | 1.6(1) | >99 |
| **6** | 6-Me-TPA | 4.2(1) | 95 | 1.6(1) | 69 | 4.1(1) | 94 | 1.1(1) | >99 |
| **7** | 6-$Me_2$-TPA | 3.9(5) | 84 | 1.3(1) | 40 | 4.8(1) | 95 | 0.6(1) | >99 |
| **8a** | 6-$Me_3$-TPA | 4.1(4) | 93 | 0.4(1) | 35 | 3.8(6) | 96 | 0.3(1) | >99 |
| **8d** | 6-$Me_3$-TPA, $O_2CC_6H_4$-3-$NO_2$ | 4.5(2) | 97 | 0.4(1) | 0 | 5.3(1) | >99 | 0.2(1) | >99 |

[a] See Experimental Section for reaction conditions. [b] Yields expressed in moles of product per mole of iron. [c] RC, the percentage of retention of configuration in the dihydroxylation and in the epoxidation of 2-heptenes, expressed as the ratio of the diols or the epoxides: 100(cis − trans)/(cis + trans) for *cis*-olefin oxidation and 100(trans − cis)/(cis + trans) for *trans*-olefin oxidation.

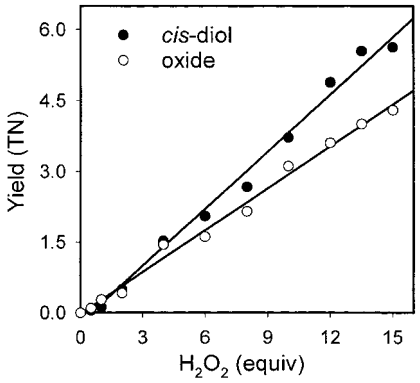


***Figure 3.*** Yields of epoxide and *cis*-diol products as a function of the amount of $H_2O_2$ added for the oxidation of cyclooctene by **4**.

a radical cation species,[42,43] and the amount of PhCHO formed decreases significantly when styrene oxidation is carried out under Ar.

**Formation of an $Fe^{III}$−OOH Intermediate.** More detailed studies of olefin oxidation catalyzed by **4** provide insights into the nature of the metal species involved. Figure 3 shows the oxidation of cyclooctene monitored as a function of added $H_2O_2$. For **4**, the amounts of *cis*-diol and oxide products increase linearly with increasing amounts of $H_2O_2$, and the diol/epoxide ratio is maintained. These results support the notion that *cis*-diol and epoxide are produced by related but independent pathways, the partitioning between which is controlled by the nature of the tetradentate ligand. However, no organic products are detected upon the addition of the first 0.5 equiv of $H_2O_2$, as also noted in our study of alkane hydroxylation by **4**/$H_2O_2$.[22] This lag in product formation is rationalized by the prior oxidation of the $Fe^{II}$ complex to the catalytically active $Fe^{III}$ species, which would consume only 0.5 equiv of $H_2O_2$. Once formed, the active $Fe^{III}$ catalyst reacts with more $H_2O_2$ to generate the olefin oxidation products. Consistent with this required preoxidation for the iron(II) catalyst, no lag phase is observed in product formation when $[Fe^{III}_2O(TPA)_2(H_2O)_2](ClO_4)_4$ (**4a**) is used in place of **4**. Complex **4a** exhibits a catalytic efficiency comparable to that of **4** and, with 10 equiv of $H_2O_2$, affords 4.1(1) TN *cis*-diol and 4.0(1) TN epoxide under the same conditions (Table 2). Thus, both **4** and **4a** act as precursors to the active oxidant for olefin oxidation. As shown in electrospray ionization mass spectrometry (ESI-MS) studies discussed below, both generate an intermediate $Fe^{III}$−OH species,[44] which in turn reacts with more $H_2O_2$ to form the active $Fe^{III}$−OOH oxidant (Scheme 1).[45]

We earlier proposed that a low-spin $Fe^{III}$−OOH intermediate is involved in catalytic alkane hydroxylation by the TPA and BPMEN families of catalysts.[22] Such species have recently been trapped and spectroscopically characterized in a number of related non-heme iron systems,[46] although pentadentate ligands were necessary in many cases in order to stabilize the intermediates sufficiently for observation. The low-spin $Fe^{III}$−

(42) Heimbrook, D. C.; Carr, S. A.; Mentzer, M. A.; Long, E. C.; Hecht, S. M. *Inorg. Chem.* **1987**, *26*, 3835−3836.
(43) Groves, J. T.; Gross, Z.; Stern, M. K. *Inorg. Chem.* **1994**, *33*, 5065−5072.

(44) The importance of an intermediate $Fe^{III}$−OH species raises the question of why iron(II) complexes are generally used as starting points for catalysis in this study instead of corresponding iron(III) complexes. Both **4** and **4a** are effective catalysts because they have ready access to the $Fe^{III}$−OH species that allows efficient formation of the key $Fe^{III}$−OOH intermediate. However, iron(III) complexes such as **4a** with an easily displaced water ligand are not readily available. Often, the high Lewis acidity of the iron(III) center leads to the formation of stable complexes with less labile ligands that inhibit the ligand exchange needed to rapidly form the $Fe^{III}$−OOH intermediate and catalyze $H_2O_2$ disproportionation instead. Such ligand differences have also been shown to affect the course of alkane hydroxylation by non-heme iron complexes.[22,45]
(45) Mekmouche, Y.; Ménage, S.; Toia-Duboc, C.; Fontecave, M.; Galey, J.-B.; Lebrun, C.; Pecaut, J. *Angew. Chem., Int. Ed.* **2001**, *40*, 949−952.
(46) Girerd, J.-J.; Banse, F.; Simaan, A. J. *Struct. Bonding* **2000**, *97*, 143−177.

***Scheme 1.*** Formation of an $Fe^{III}$ −OOH Intermediate

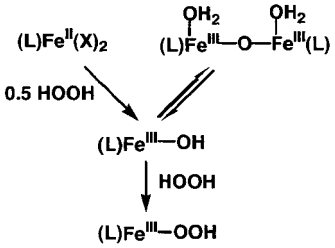


OOH intermediate for **4**, albeit less stable than its pentadentate ligand counterparts, has been observed at −40 °C and found to have a $\nu$(O−O) near 800 $cm^{-1}$,[47] a value comparable to those observed for other low-spin $Fe^{III}$−OOH intermediates but significantly lower than those observed for high-spin $Fe^{III}$−peroxo complexes.[29,46,48,49] Thus, the low-spin iron(III) center weakens the O−O bond and activates it for cleavage.[25,47] Since the conditions for alkane hydroxylation and olefin oxidation are identical save for the nature of the substrates, it seems reasonable to postulate the involvement of this intermediate in olefin oxidation.

ESI-MS has proven to be an excellent tool for establishing the molecular compositions of transient species in iron-catalyzed oxidations.[33] Its utility is illustrated for the reactions of the TPA catalyst. When the effluent derived from combining precooled solutions of **4** or **4a** and $H_2O_2$ in a mixing tee is introduced directly into the mass spectrometer, two signals are observed in the positive ion mass spectrum at *m*/*z* 462 and 478 (Figure 4A). The *m*/*z* 462 signal has a mass and isotope distribution pattern that corresponds to $\{[Fe^{III}(TPA)(OH)](ClO_4)\}^+$, which is the precursor to the species that gives rise to the prominent signal at *m*/*z* 478. The latter has a mass value and an isotope distribution pattern consistent with its formulation as $\{[Fe^{III}(TPA)(OOH)](ClO_4)\}^+$. MS/MS experiments show that the fragmentation of the *m*/*z* 478 ion gives rise to a prominent daughter ion at *m*/*z* 445 due to the loss of OOH forming $\{[Fe^{II}(TPA)](ClO_4)\}^+$ and a much weaker daughter ion at *m*/*z* 461, corresponding to the loss of OH forming $\{[Fe^{IV}(TPA)(O)](ClO_4)\}^+$. Last there is also a molecular ion signal in the negative ion mass spectrum at *m*/*z* 676 corresponding to the ion $\{[Fe^{III}(TPA)(OOH)](ClO_4)_3\}^-$ (data not shown).

Notably, the molecular ion at *m*/*z* 478 of the Fe−OOH species is not affected by the presence of $H_2{}^{18}O$. This result shows that the peroxo oxygen atoms in this ion do not exchange with water and that the O−O bond remains intact at this stage of the characterization, as expected. The mass spectral data unfortunately do not provide any insight as to the identity of the sixth ligand, which would very likely be required to achieve the low-spin iron(III) state indicated by the EPR spectrum of the intermediate.[25] Considering the readily dissociable nature of this ligand, we presume that the sixth coordination site is occupied by a labile solvent molecule such as $CH_3CN$ or $H_2O$.

New species are observed in the ESI-MS spectra of the $Fe^{III}$−OOH intermediate generated from **4** and $H_2O_2$ in the presence of styrene. Figure 4B shows the appearance of four new signals

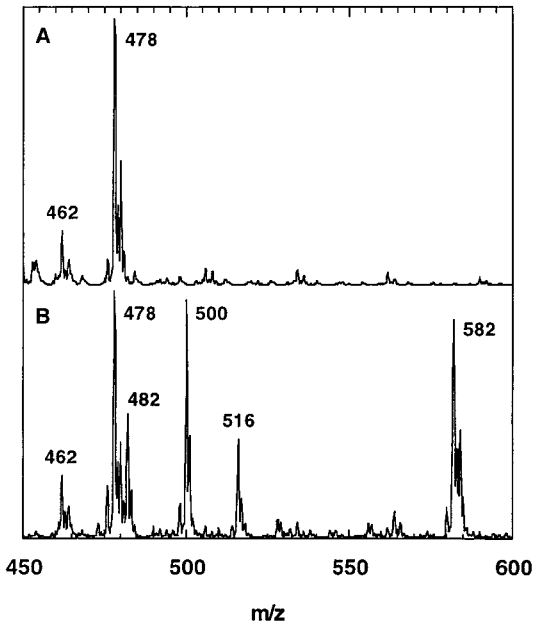


***Figure 4.*** Electrospray ionization mass spectra for the reaction of **4** with $H_2O_2$ in $CH_3CN$ at −40 °C in the absence (A) and in the presence of styrene (B).

***Chart 2.*** Proposed Structures Corresponding to the ESI-MS Ions of the Species Generated in the Reaction of **4** and $H_2O_2$ in the Presence of Styrene

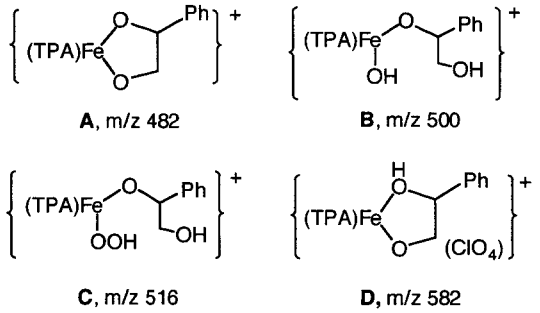


at *m*/*z* 482, 500, 516, and 582, in addition to the original features at *m*/*z* 462 and 478. The most intense of these signals at *m*/*z* 582 has a mass and an isotope distribution pattern that correspond to a combination of the $Fe^{III}$−OOH intermediate ion and styrene (*m*/*z* 478 + 104). This combination can be construed as the $\{[(TPA)Fe^{III}-OOH]\cdot styrene\cdot ClO_4\}^+$ adduct, $\{[(TPA)Fe^{III}-OH]\cdot styrene\ oxide\cdot ClO_4\}^+$, or $\{[(TPA)Fe^{III}$-styrene diolate$]ClO_4\}^+$. The MS/MS experiment on this ion shows that its fragmentation generates only one major daughter ion at *m*/*z* 482 due to the loss of $HClO_4$ (Figure S1c, Supporting Information). The fact that there is no daughter ion due to the loss of styrene alone suggests that the styrene and OOH components have already combined chemically. Since there is also no daughter ion due to the loss of styrene oxide alone, it is reasonable then to formulate the *m*/*z* 582 ion as the complex of the diol product (structure **D** in Chart 2). The stability of this ion is not surprising, given the expected bidentate coordination of the diol to the iron center and the oxophilicity of iron(III). The assignment of the *m*/*z* 482 ion to structure **A** in Chart 2 can be rationalized on the same basis. The ions at *m*/*z* 500 and 516 both fragment by loss of diol and respective losses of $H_2O$ and OOH (Figure S1a and b, Supporting Information) and are thus formulated as structures **B** and **C** in Chart 2, respectively.

(47) Ho, R. Y. N.; Roelfes, G.; Feringa, B. L.; Que, L., Jr. *J. Am. Chem. Soc.* **1999**, *121*, 264−265.
(48) Lehnert, N.; Ho, R. Y. N.; Que, L., Jr.; Solomon, E. I. *J. Am. Chem. Soc.* **2001**, *123*, 8271−8290.
(49) Lehnert, N.; Ho, R. Y. N.; Que, L., Jr.; Solomon, E. I. *J. Am. Chem. Soc.* **2001**, *123*, 12802−12816.

***Table 6.*** Isotope Labeling Results from the Oxidation of Cyclooctene by $H_2O_2$ Catalyzed by Iron Complexes[a]

| | | cyclooctene oxide-$^{18}$O% | | | *cis*-cyclooctane-1,2-diol | | | |
|---|---|---|---|---|---|---|---|---|
| | | | | | $H_2{}^{18}O$ | | $H_2{}^{18}O_2$ | |
| | ligand | $H_2{}^{18}O$ | $H_2{}^{18}O_2$ | $^{18}O_2{}^b$ | $^{16}O^{18}O$ | $^{18}O^{18}O$ | $^{16}O^{18}O$ | $^{18}O^{18}O$ |
| **4** | TPA | 9(1) | 90(8) | 1 | 86(5) | 1(1) | 97(3) | 3(1) |
| **5** | 5-Me$_3$-TPA | 2(1) | 93(6) | 5 | 83(9) | 1(1) | 97(3) | 2(2) |
| **6** | 6-Me-TPA | 7(1) | 71(9) | 22 | 80(1) | 2(1) | 94(4) | 6(1) |
| **7** | 6-Me$_2$-TPA | 3(1) | 61(8) | 36 | 3(1) | 1(1) | 7(1) | 93(3) |
| **8a** | 6-Me$_3$-TPA | 3(1) | 54(2) | 43 | 1(1) | 0 | 4(1) | 96(1) |

[a] See Experimental Section for reaction conditions. [b] Calculated considering mass balance of the oxygen atom.

Thus, the product diol coordinates to the metal center in the course of a turnover and is presumably displaced by $H_2O_2$ to initiate the next round of catalysis.

**$^{18}$O-Labeling Experiments.** The subsequent fate of the bound hydroperoxide has been probed by $^{18}$O-labeling experiments for the TPA series of catalysts, and these studies provide key insights into the nature of the oxidants in the mechanisms for olefin oxidation (Table 6). As for the previously reported alkane hydroxylation experiments,[22,28] oxidations were carried out in the presence of added water to determine the source(s) of the oxygen atom(s) incorporated into the epoxide and *cis*-diol products. The presence of the added water does not significantly affect the product yields observed for the various catalysts in this study.

The epoxidation of cyclooctene with $H_2{}^{18}O_2$ in the presence of 1000 equiv of $H_2{}^{16}O$ catalyzed by **4** affords the corresponding epoxide with 90% incorporation of the $^{18}$O label. When $H_2{}^{16}O_2$ is used in the presence of 1000 equiv of $H_2{}^{18}O$, the complementary result is obtained with 9% of the epoxide $^{18}$O-labeled. Thus, all the oxygen present in the epoxide derives either from $H_2O_2$ or from the $H_2O$ present in the solution, with essentially no incorporation of $O_2$ from air into the epoxide due to autoxidation. The same results are obtained for **5**. Thus, the incorporation of $^{18}$O from $H_2{}^{18}O$ into the epoxide products requires the participation of an oxidant capable of solvent water exchange in the epoxidation mechanism.

The extent of $^{18}$O incorporation into the epoxide product from various oxygen sources is affected by the number of 6-Me substituents on the pyridine ligands (Table 6). For **6** with one 6-Me substituent, the epoxide product derives its oxygen atom 71% from $H_2O_2$ and 7% from $H_2O$, with the remaining 22% presumably from air. No $^{18}$O from $H_2{}^{18}O$ is incorporated into epoxide products of **7** and **8a**, complexes with two or three 6-Me substituents, and the percentage incorporation from $H_2O_2$ also decreases to ~60%, so the presumed contribution from air increases to ~40% (Table 6). In fact, the increase in percent O from $O_2$ in cyclooctene epoxidation correlates well with the decrease in RC value in the epoxidation of *cis*-2-heptene, as shown in Figure 5. This linear correlation suggests an increased involvement of a radical cation intermediate leading to epimerization and autoxidation in the mechanism of olefin epoxidation as the number of 6-methyl substituents increases. This trend parallels the observations we reported previously for alkane hydroxylation by this family of catalysts, where increasing the number of 6-methyl substituents causes a decrease in the stereospecificity in the hydroxylation of *cis*-1,2-dimethylcyclohexane and an increase in the percent O derived from $O_2$ into the alcohol product.[22]

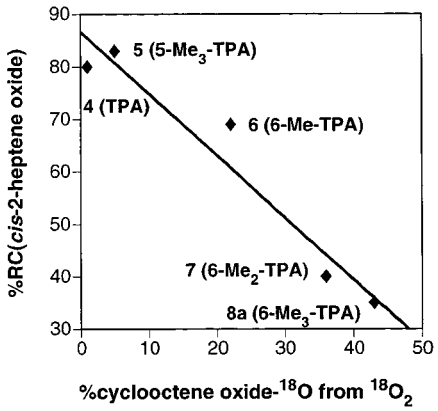


***Figure 5.*** Linear correlation between the RC value for *cis*-2-heptene epoxidation and the amount of $O_2$ incorporation into cyclooctene oxide for the TPA series of catalysts ($r^2 = 0.94$). Data obtained from Tables 5 and 6.

Quite distinct from the isotope labeling results for epoxidation are those for *cis*-diol formation (Table 6), emphasizing the notion that cis-dihydroxylation operates by a parallel but independent mechanism. Both oxygen atoms of the *cis*-diol obtained from **7**- and **8a**-catalyzed oxidations derive essentially from $H_2O_2$, with no incorporation of isotope label from the addition of 1000 equiv of $H_2{}^{18}O$. As previously reported,[26] a labeling experiment with a 60:40 mixture of $H_2{}^{16}O_2$ and $H_2{}^{18}O_2$ in the oxidation of cyclooctene by **8a** afforded a 60:40 ratio of unlabeled and doubly labeled *cis*-diol and a negligible amount of the $^{16}O^{18}O$ isotopomer. This experiment demonstrates that the diol oxygens in **8a**-catalyzed cis-dihydroxylation derive from one molecule of $H_2O_2$.

Dramatically different isotopic labeling results are obtained for cis-dihydroxylation by **4**, **5**, and **6**, catalysts with either no 6-Me substituent or only one 6-Me substituent (Table 6). In these cases, only one of the oxygen atoms of the *cis*-diol becomes isotopically labeled either from experiments carried out with $H_2{}^{16}O_2$ in the presence of 1000 equiv of $H_2{}^{18}O$ or from the complementary reactions with $H_2{}^{18}O_2$ and 1000 equiv of $H_2{}^{16}O$. Thus, one oxygen atom of the *cis*-diol derives from $H_2O_2$, while the other derives from $H_2O$. These observations require a mechanism involving an oxidizing species that can fully equilibrate with solvent water.

$^{18}$O incorporation from $H_2{}^{18}O$ into the epoxide and *cis*-diol products of **4** display saturation behavior (Figure 6), as shown previously for **5**-catalyzed hydroxylation of cyclohexane with $H_2O_2$.[22] This behavior indicates a preequilibrium binding of water to the metal center during turnover. Double-reciprocal plots of the data (Figure 6 insets) in fact show straight lines that give estimated association constants of about 20 and 30 $M^{-1}$, respectively, values that are comparable to the 16 $M^{-1}$ value obtained in the cyclohexane hydroxylation study.[22] This congruence in the isotope labeling results suggests that the same water binding equilibrium affects the oxidizing species involved in Fe(TPA)-catalyzed alkane hydroxylation, olefin epoxidation, and olefin cis-dihydroxylation.

**Mechanistic Considerations.** Scheme 2 shows the proposed mechanism for olefin epoxidation and cis-dihydroxylation catalyzed by the family of non-heme iron complexes discussed here. These olefin oxidation studies build on the foundation provided by our earlier work on alkane hydroxylation by this same family of catalysts[22] and further validate key features of

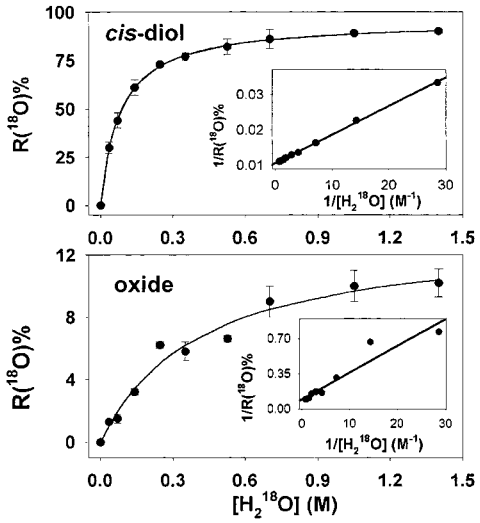


***Figure 6.*** Fraction of $^{18}$O-labeled *cis*-diol (top) and epoxide (bottom) obtained in the oxidation of cyclooctene catalyzed by **4**/$H_2O_2$ as a function of the concentration of $H_2{}^{18}O$ ($[H_2{}^{18}O]$). Insets: the double-reciprocal plots.

***Scheme 2.*** Proposed Mechanism for Catalysis

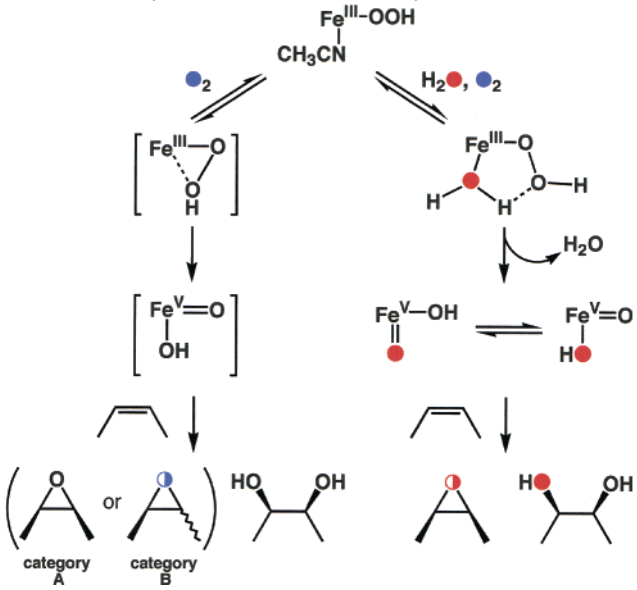


a mechanism that posits the participation of an $Fe^{III}$—OOH intermediate and the corresponding $Fe^{V}$=O derivative. The proposed mechanism takes into account the following observations:

1. Only complexes with two cis labile sites are effective catalysts for olefin epoxidation and cis-dihydroxylation.

2. Category A complexes, with ligands having either no 6-methyl substituent (**1**, **2**, **4, 5**) or only one 6-methyl substituent (**6**), catalyze highly stereoselective olefin epoxidation and olefin cis-dihydroxylation. Epoxide and *cis*-diol products incorporate $^{18}$O from $H_2{}^{18}O$ via an $[H_2{}^{18}O]$-dependent preequilibrium.

3. Category B complexes, with ligands having more than one 6-methyl substituent (**3**, **7**, **8a**−**d**), catalyze olefin cis-dihydroxylation predominantly, affording *cis*-diols with both oxygen atoms derived from $H_2O_2$.

As proposed in our alkane hydroxylation studies,[22] what distinguishes category A catalysts from those in category B is the spin state of the $Fe^{III}$—OOH intermediate, which can be tuned by the number of 6-methyl substituents on the tripodal ligand, as precedented by the $[Fe^{III}(6\text{-Me}_x\text{-TPA})(OO^tBu)]^{2+}$ series ($x$ = 0−3).[29]

Category A complexes (**1**, **2**, **4**, **5**, **6**) afford low-spin $Fe^{III}$—OOH intermediates, whose O—O bonds are weakened by the presence of the $S = {}^1/_2$ iron center.[47] The fact that **9**, with the closely related but pentadentate N4Py ligand, also forms a similar low-spin $Fe^{III}$—OOH intermediate[47] but is not a catalyst for olefin oxidation[26] suggests that the presence of the low-spin iron(III) center is insufficient to account for the reactivity observed. The adjacent second labile site on the catalyst must thus serve a critical role in activating the bound peroxide.

In the right branch of Scheme 2, we propose that peroxide activation occurs by preequilibrium water binding to the adjacent labile site of the $Fe^{III}$—OOH intermediate. A five-membered ring species is formed that promotes O—O bond heterolysis to generate the *cis*-$H^{18}O$—$Fe^{V}$=O oxidant. The observation of $^{18}$O incorporation from $H_2{}^{18}O$ into the epoxide and *cis*-diol products of these reactions strongly supports this mechanistic hypothesis, as it requires another intermediate that is capable of solvent water exchange. Partial labeling of the epoxide product with $^{18}$O from $H_2{}^{18}O$ would occur by oxo−hydroxo tautomerism of the *cis*-$H^{18}O$—$Fe^{V}$=O oxidant, as precedented in heme systems,[50,51] which would introduce $^{18}$O into the terminal iron−oxo unit before oxygen atom transfer to the olefinic substrate. Cis-dihydroxylation, on the other hand, entails the transfer of two oxygen atoms from oxidant to substrate. Thus, the observation that one oxygen atom of the *cis*-diol product derives from $H_2O$ while the other comes from $H_2O_2$ strongly supports the involvement of the proposed *cis*-$H^{18}O$—$Fe^{V}$=O species; it in fact represents the strongest evidence that the *cis*-$H^{18}O$—$Fe^{V}$=O species is the oxidant for category A catalysts in the presence of excess water.

The mechanism shown on the right branch of Scheme 2 may apply as well for category A catalysts in the absence of excess water, but we cannot exclude the mechanism shown on the left branch. In this case, the $Fe^{III}$-$\eta^1$-OOH intermediate would be activated by isomerization to an $\eta^2$-OOH species, which may either react directly with the olefin or convert to the high-valent species prior to attack of the olefin. In such a pathway, the highly stereoselective epoxide and *cis*-diol products derive their oxygen atoms exclusively from $H_2O_2$. The less than 10% incorporation of $^{18}$O from $H_2{}^{18}O$ into the epoxide may argue for the involvement of both branches of Scheme 2 for category A catalysts, but the high level of $^{18}$O incorporation into the *cis*-diol shows that the right branch of Scheme 2 dominates for cis-dihydroxylation.

Category B catalysts (**3**, **7**, **8a**−**d**), on the other hand, very likely give rise to high-spin $Fe^{III}$—OOH species due to the steric effects of the 6-methyl substituents.[29] The lack of $^{18}$O incorporation from $H_2{}^{18}O$ into epoxide and *cis*-diol products excludes the right branch of Scheme 2 as the mechanism for peroxide activation. Consistent with the alternative mechanism on the left branch, both diol oxygens of the *cis*-diol products derive almost exclusively from $H_2O_2$. At present, it is not clear why category B catalysts should strongly favor olefin cis-dihydroxylation, but our data unequivocally establish this preference. Furthermore, unlike for category A catalysts, category B catalysts yield minor epoxide products with significant loss of

(50) Bernadou, J.; Meunier, B. *Chem. Commun.* **1998**, 2167−2173.
(51) Meunier, B.; Bernadou, J. *Struct. Bonding* **2000**, *97*, 1−35.

stereochemistry and incorporation of oxygen from $O_2$. Instead of a mechanism involving direct oxygen atom transfer, these observations strongly suggest a stepwise epoxidation mechanism involving the initial oxidation of olefin to a radical cation intermediate. Thus, the reactivity of high-spin $Fe^{III}-OOH$ species differs significantly from that of their low-spin counterparts.

Scheme 2 represents our best working model to date for our family of catalysts. There is strong evidence for $Fe^{III}-OOH$ intermediates as well as the participation of a *cis*-$HO-Fe^{V}=O$ oxidant in category A reactions, but not for the intermediates shown in brackets; these various reactive species, however plausible, are at present all speculations based on detailed product analysis and $^{18}O$ labeling. Kinetic studies may also contribute to our understanding of the mechanism. However, the syringe pump conditions used in this study are not conducive for the demonstration of a particular rate law, since $H_2O_2$ concentrations are maintained at a level substoichiometric relative to catalyst in order to minimize deleterious side reactions and maximize $H_2O_2$ conversion into the desired products.

**Summary and Perspectives.** In this paper, we have characterized a family of non-heme iron catalysts with two cis labile sites, which are capable of stereospecific olefin epoxidation and cis-dihydroxylation using $H_2O_2$ as oxidant. Ligand tuning of the spin state of the $Fe^{III}-OOH$ species formed in the course of catalysis results in the range of reactivities observed. A dramatic illustration of this effect can be seen in the BPMEN series, where a 32-fold change in the *cis*-diol/epoxide ratio is observed on going from **1**, which catalyzes epoxidation almost exclusively (89% of the total products), to **3**, which favors cis-dihydroxylation (80% of the total products).

The complexes in this series are in fact the first examples of iron catalysts capable of olefin cis-dihydroxylation, thus providing a unique opportunity to gain insight into its novel mechanism. Category A catalysts give rise to low-spin $Fe^{III}-OOH$ intermediates and afford *cis*-diol products that incorporate one oxygen atom from $H_2O_2$ and the other from $H_2O$. Taken together with the observation that alkane hydroxylation and olefin epoxidation products also incorporate $^{18}O$ from $H_2{}^{18}O$, these results provide compelling evidence for a *cis*-$H^{18}O-Fe^{V}=O$ species as the common oxidant in these reactions (Scheme 2 right). Category B catalysts, on the other hand, give rise to high-spin $Fe^{III}-OOH$ intermediates and afford *cis*-diol products with both oxygen atoms from $H_2O_2$. Activation of the O−O bond is proposed to occur via an $Fe^{III}$-$\eta^2$-OOH species that may isomerize into a *cis*-$HO-Fe^{V}=O$ species in the course of catalysis (Scheme 2 left).

Our studies provide a basis with which to rationalize Nature's choice of ligand environments for carrying out iron-catalyzed alkene oxidations. Olefin epoxidation is carried out by cytochrome P450 and the non-heme iron-requiring antitumor drug bleomycin; their metal centers have only one available site with which to form low-spin $Fe^{III}-OOH$ intermediates.[16,52,53] Without an adjacent labile site, such intermediates can only give rise to olefin epoxidation.

On the other hand, cis-dihydroxylation of C−C double bonds is catalyzed only by bacterial non-heme iron Rieske dioxygenases.[5] These enzymes have a mononuclear iron site that is coordinated to two histidine imidazoles and a bidentate carboxylate from aspartate[19] with two cis sites available for exogenous ligand binding. Our model studies suggest that olefin cis-dihydroxylation is favored by a high-spin iron center with two cis labile sites. Given the weak crystal field expected from the 2-His-1-carboxylate facial triad,[54] it seems likely that the proposed but as yet unobserved iron(III)−hydroperoxo intermediate in the catalytic cycle of these enzymes will have a high-spin state. Furthermore, there are two cis labile sites available for activating the bound hydroperoxide to the putative *cis*-$HO-Fe^{V}=O$ species. Evidence is unavailable for the participation of such a high-valent species in cis-dihydroxylation by the enzymes, since $^{18}O$-labeling studies show that both atoms of $O_2$ are incorporated into the *cis*-diol product. However, $^{18}O$ from $H_2{}^{18}O$ is found in the alcohol product of the highly enantioselective hydroxylation of indane by toluene and naphthalene dioxygenases,[55,56] so an $Fe^{V}=O$ species can form in the Rieske dioxygenase active site and may thus be involved in cis-dihydroxylation as well. The insights we have gained in the foregoing study illustrate the utility of biomimetic investigations to shed light on biological mechanisms for oxygen activation.

**Acknowledgment.** This work was supported by the National Institutes of Health (GM-33162). K.C. is grateful to a thesis fellowship from the Department of Chemistry of the University of Minnesota. M.C. acknowledges the Fundacio La Caixa for a fellowship. The authors thank Dr. Victor G. Young, Jr., and Dr. Maren Pink (X-ray Crystallographic Laboratory, University of Minnesota) for solving the crystal structures of complexes **2** and **3**.

**Supporting Information Available:** Table S1 of the crystallographic data of **2** and **3**, Figure S1 of MS/MS spectra of ions obtained from the precooled mixture of **4** or **4a** and $H_2O_2$ in the presence of styrene, and X-ray crystallographic data for **2** and **3** (CIF). This material is available free of charge via the Internet at http://pubs.acs.org.

JA0120025

(52) Davydov, R.; Makris, T. M.; Kofman, V.; Werst, D. E.; Sligar, S. G.; Hoffman, B. M. *J. Am. Chem. Soc.* **2001**, *123*, 1403−1415.
(53) Burger, R. M.; Kent, T. A.; Horwitz, S. B.; Münck, E.; Peisach, J. *J. Biol. Chem.* **1983**, *258*, 1559−1564.
(54) Hegg, E. L.; Que, L., Jr. *Eur. J. Biochem.* **1997**, *250*, 625−629.
(55) Wackett, L. P.; Kwart, L. D.; Gibson, D. T. *Biochemistry* **1988**, *27*, 1360−1367.
(56) Gibson, D. T.; Resnick, S. M.; Lee, K.; Brand, J. M.; Torok, D. S.; Wackett, L. P.; Schocken, M. J.; Haigler, B. E. *J. Bacteriol.* **1995**, *177*, 2615−2621.